Admittance spectroscopy study of polymer diodes in small magnetic fields

Thaddee K. Djidjou, Tek Basel, and Andrey Rogachev
Department of Physics and Astronomy, University of Utah, Salt Lake City, Utah 84112, USA

(Received 7 May 2012; accepted 20 June 2012; published online 20 July 2012)

We performed a systematic study of bipolar and unipolar organic diodes based on the π-conjugated polymer, 2-methoxy-5-(2′-ethylhexyloxy) (MEH-PPV), using electronic and magneto-transport measurements with magnetic field in the range 0–180 mT and admittance spectroscopy in the frequency range 1 Hz $< f <$ 10 MHz. The admittance spectra of bipolar devices reveal two relaxation processes with distinct time scales that are influenced by the magnetic field. The slower process, which dominates the device capacitance at $f <$ 10 Hz, is attributed to the trap-assisted monomolecular recombination. The faster process is attributed to the electron-hole bimolecular recombination kinetics. We found that the time scale of this process, τ_2, decreases exponentially with the bias voltage. Application of magnetic field, $B = 30$ mT decreases τ_2 by ∼30%. We also found that the magneto-conductance, $\Delta G(\omega, B)/G(\omega, 0)$, has a characteristic cutoff frequency that shifts to higher frequencies with increasing bias voltage. In particular, the magnetoconductance at 10 MHz in a *bipolar device* was measured to be 4.5% at $B = 30$ mT. For bipolar devices we found that the frequency-dependent response of the device admittance to the small magnetic field is identical to the response of the admittance to a small increase in the bias voltage in zero magnetic field. We also found that the admittance of *unipolar diodes* does not depend on magnetic field. © *2012 American Institute of Physics*. [http://dx.doi.org/10.1063/1.4737773]

INTRODUCTION

Large magnetoresistance has been recently observed in organic semiconductor diodes with no ferromagnetic electrodes. This effect is referred to as organic magnetoresistance (OMAR); it reaches sizable value of 20% in relatively small field of order 10 mT at room temperature.[1–3] OMAR is strongest in bipolar devices, but it was also detected in unipolar devices with both electron and hole carriers.[4] Several mechanisms have been proposed to explain the OMAR; however, none of them can account for the whole body of the experimental observations. The models consider the effect of magnetic field on various electronic and spin-related processes in the organic interlayer of the devices, such as bipolaron formation,[5] singlet to triplet interconversion in electrostatically bound electron-hole pairs,[6,7] and detrapping of charges by triplet excitons.[8] Most of these models are based on the hyperfine interaction (HFI) between the injected spin $^1/_2$ carriers and nuclear spins in the organic active layer. Recently by replacing protons with deuterons (that have smaller HFI constant) in an organic polymer interlayer it was demonstrated that indeed the HFI plays a crucial role in the OMAR effect.[9] It is possible that in some organic materials several magnetic-field-dependent processes occur concurrently. Experimental discrimination between different mechanisms typically involves analysis of the DC current response versus magnetic field, $I(B)$. It is desirable to extend the study of OMAR effect beyond the DC transport measurements. In several recent experiments, the response of organic light emitting diodes (OLED) to an alternating magnetic field has been studied. A characteristic frequency cutoff of the OMAR effect observed in these experiments was attributed to the transient time of minority carriers.[10] However, this conclusion has not been confirmed in later work.[11] The effect of magnetic field on the time evolution of the device current following application of a voltage pulse has also been studied.[12] It was concluded that the magnetic field may increase electron-hole recombination rate, but has no effect on the carriers' mobility. In the presented work, we report on the effect of the magnetic field on the complex admittance of organic semiconductor devices in the frequency range 1 Hz–10 MHz. With this method, we identify two magnetic-field-dependent processes that occur concurrently in bipolar diodes.

EXPERIMENTAL

Bipolar OLEDs were fabricated on glass substrates in cross-bar geometry. The devices with surface area of about 1 mm^2 consist of multilayers having the structure ITO/PEDOT:PSS/MEH-PPV/Ca/Al. The multilayers are indium tin oxide (ITO) that is a transparent anode; PEDOT:PSS, poly(3,4-ethylenedioxythophene):poly(styrene sulphonate) that forms a hole injection layer; the active layer was the generic π-conjugated polymer 2-methoxy-5 -(2′-ethylhexyloxy) (MEH-PPV). The cathode was a 2 nm-thick Ca layer covered by an Al layer for oxidation protection. The unipolar (hole carriers) devices had similar geometry with the structure ITO/PEDOT:PSS/MEH-PPV/Au. The devices were sealed with a glass slide to provide protection against oxidation. The transport measurements were carried out at ambient conditions. The devices slowly degraded over time, but were suitable for the transport measurements for several days. Because of the slow degradation, we carried out overlapping series of measurements on several devices. Overall 14 devices were studied; data for five of them are used in this contribution. Device A is a bipolar diode with MEH-PPV thickness of ∼80 nm. Devices B, C, and D are bipolar

diodes with MEH-PPV thickness of ~150 nm. Device E is a unipolar diode with MEH-PPV thickness ~150 nm.

The admittance spectroscopy measurements were performed at room temperature using a home-made apparatus. The calibrations and measurements were performed following the procedures outlined in Ref. 13. The distance between the sample and the front operational amplifier (works as a current to voltage converter) was very short (5 mm), which significantly decreases the system stray capacitance. In a typical experiment, the device was subjected to a DC bias voltage, V_B, superimposed with a small AC voltage with an amplitude of 10–20 mV and frequency of 1 Hz–10 MHz. In-phase and quadrature components of the AC current were detected using phase sensitive techniques and used to calculate the complex admittance of the device. For the transport measurements in magnetic field, the OLEDs were positioned between poles of an electromagnet, with magnetic field up to 180 mT.

RESULTS AND DISCUSSION

In Fig. 1, we show current vs. voltage, $I(V)$, characteristics of two extensively studied MEH-PPV devices: bipolar device B and unipolar device E. The inset in Fig. 1(a) shows a schematic band diagram of the bipolar device with indicated HOMO-LUMO of the MEH-PPV polymer,[14] and work functions of Ca (Ref. 14) and PEDOT:PSS (Ref. 15). The $I(V)$ characteristics in organic diodes based on π-conjugated polymers often take the form $I \propto V^n$. The exponent, n, can be directly determined from the obtained data by the relation: $n = d(\ln(I))/d(\ln(V))$. The parameter n thus determined is also plotted in Fig. 1; $n(V)$ is not constant in both devices. Figure 1(b) shows $I(V)$ and $n(V)$ for a unipolar device E. Here we can identify three regimes: ohmic regime with $n = 1$ at $V_B < 0.7$ V, space charge limited regime with $I \propto V^2$ at $V_B > 5$ V, and a transitional trap-filling regime at intermediate bias voltages. Similar $I(V)$ characteristics for unipolar MEH-PPV diodes were reported in Ref. 16.

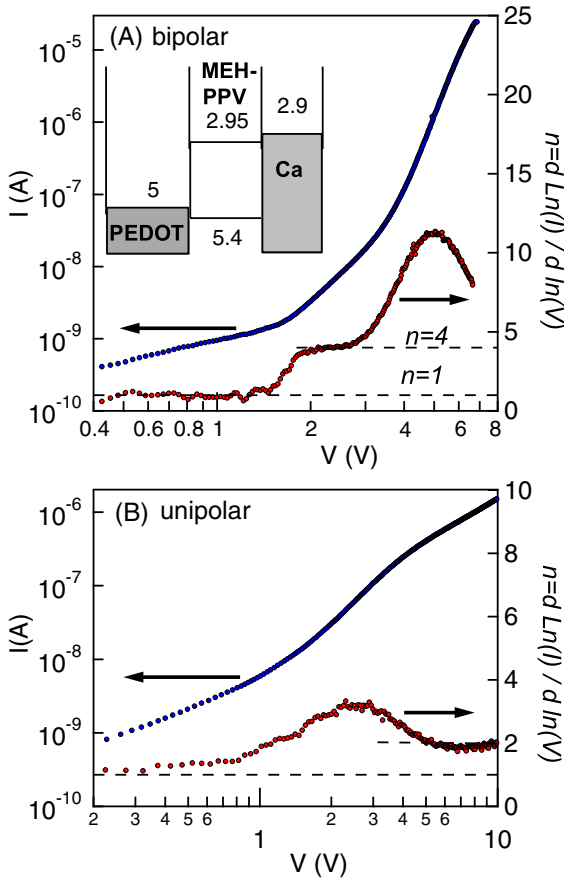

FIG. 1. Current-voltage characteristics (blue dots, left axis) of bipolar MEH-PPV diode B (panel (a)) and unipolar device E (panel (b)). The voltage dependence of the exponent n in $I \propto V^n$ is also shown (red dots, right axis). Plateaus with $n = 1$, 2 and $n = 4$ are indicated by dashed lines. The inset in (a) schematically shows the important energy levels associated with a bipolar device.

At low bias the bipolar device (Fig. 1(a)) is in the ohmic regime, where $n = 1$. Once the bias voltage exceeds the built-in potential, V_{BI} (≈2 V), the carrier injection into the MEH-PPV interlayer becomes operative. We note that $n \approx 4$ in the range $2 < V_B < 3$ V. The exponent $n > 2$ indicates the presence of trap-limited regime. In MEH-PPV, the transport of both electrons and holes is affected by traps. Recent analysis of transport in an electron only unipolar MEH-PPV device suggested the presence of a Gaussian trap distribution located ~0.7 eV below the LUMO. The total density of traps was estimated to be $N_t = 1 \times 10^{23}$ m^{-3}; whereas the width of the trap energy distribution was determined to be $\sigma_t = 0.1$ eV.[17] The exponent n for trap-mediated transport having a Gaussian density of states distribution can be calculated from the equation (Eq. (3.61) in Ref. 18),

$$n = 1 + \left(1 + \frac{2}{\pi}\frac{\sigma_t^2}{16k^2T^2}\right)^{1/2}. \quad (1)$$

At room temperature and with $\sigma_t = 0.1$ eV, Eq. (1) gives $n \approx 3.6$, which is close to n obtained in the experiment for $2 < V < 3$ V. When $V_B > 3$ V, the exponent n strongly increases with voltage. This corresponds to the regime of bipolar injection. In fact, an exponential dependence of the current was recently reported for MEH-PPV-based organic light emitting diodes.[19] At high injection level, in the space-charge limited regime, the relation $I \propto V^n$ is expected with n in the range 2–3 depending on the relative strength of the bimolecular or trap mediated recombination processes.[18] There is a tendency of approaching this regime in our MEH-PPV devices at $V_B > 5$ V.

Figure 2 shows the magneto-conductance response, $MI(B)$, defined as $\Delta I(B)/I(0) = I(B)/I(0) - 1$, in bipolar device C at several bias voltages. The $MI(B)$ response can be fitted reasonably well using an empirical expression,[2,20]

$$\frac{\Delta I(B)}{I(0)} = \Delta I_0 \frac{B^2}{(|B| + B_0)^2}. \quad (2)$$

The parameter B_0 that characterizes the $MI(B)$ response line width was determined to be $B_0 = 2.5$ mT; it is somewhat smaller than a previously obtained value in thinner MEH-PPV bipolar devices.[20] It is also seen that the $MI(B)$ value at $B = 60$ mT initially increases with bias voltage, reaches a maximum value at $V_B \approx 5$ V, and decreases at higher V_B.

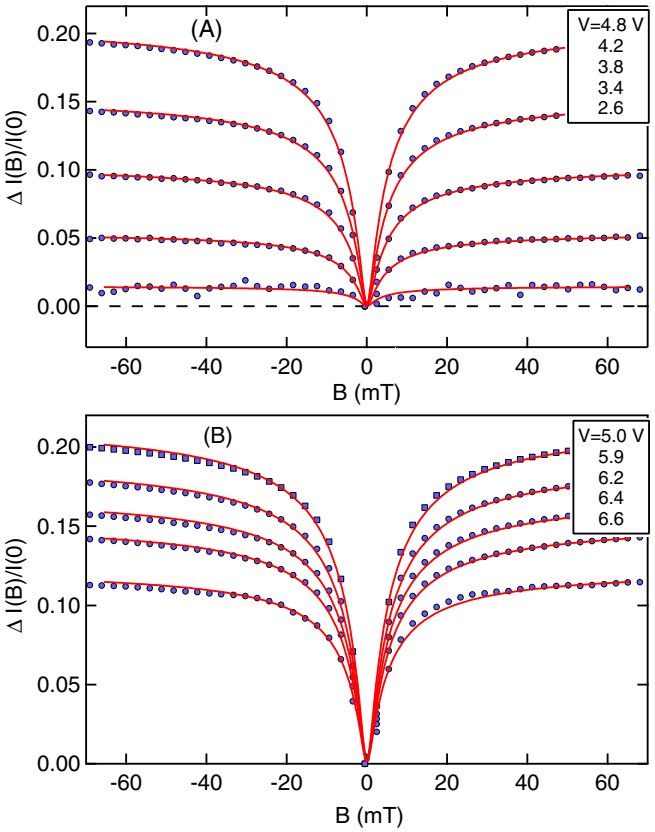

FIG. 2. The magneto-conductance $MI(B)$ response for bipolar device C at various bias voltages as indicated.

We also found that the parameter B_0 increases with V_B in agreement with the literature.[9]

The device admittance is commonly analyzed as

$$Y(\omega) = G(\omega) + i\omega C(\omega), \tag{3}$$

where $G(\omega)$ is the frequency-dependent differential conductance and $C(\omega)$ is the frequency-dependent differential capacitance. To characterize the effect of magnetic field on the device admittance we introduce two quantities: magnetoconductance $MG(\omega, B)$, defined as $\Delta G(B,\omega)/G(0,\omega) = G(B,\omega)/G(0,\omega) - 1$, and magnetocapacitance $MC(\omega, B)$, defined as $\Delta C(B,\omega)/C(0,\omega) = C(B,\omega)/C(0,\omega) - 1$. We found that both quantities, $MG(\omega, B)$ and $MC(\omega, B)$, have a non-trivial dependence on the bias voltage and frequency. For example, as shown in Fig. 3(b) for device D at $V_B = 5$ V, MC at frequencies 1000 and 1 Hz have higher magnitude than at frequencies 157 and 631 Hz. However, the magnetic field response of MG and MC was always qualitatively similar to the DC $MI(B)$ response having a characteristic saturation at $B \approx 30$ mT.

In Fig. 4(a), we show the differential conductance of device B as a function of frequency at several bias voltages. At each frequency, the conductance was measured at 0 and 30 mT with waiting time of 2 s. This procedure ensures that the magnetic field effects are not due to drift in the device characteristics. We note that the data were obtained from the measured admittance by subtracting a contribution of an in-series resistance of 36 Ω that originates from the ITO and Al

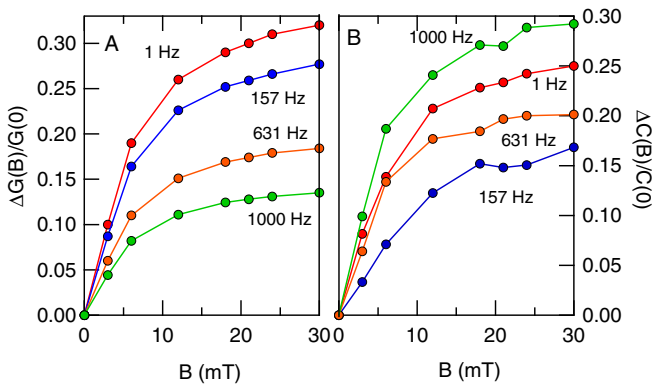

FIG. 3. The magnetoconductance (a) and the magnetocapacitance (b) response at various frequencies. The measurements were done on a bipolar device D, at bias voltage 5 V.

cross-bar electrodes. At zero bias the device conductance G strongly increases at high frequencies; similar behavior was also observed in OC_1C_{10}-PPV,[21] where it was attributed to the presence of permanent electrical dipoles in the organic material.[22] If the dipoles' response is characterized by a distribution of relaxation times, then the dielectric constant can be described by the empirical Cole-Cole equation (Eq. (9.48) in Ref. 23),

$$\frac{\varepsilon(\omega)}{\varepsilon_0} = \varepsilon_\infty + \frac{\varepsilon_s - \varepsilon_\infty}{1 + (i\omega\tau_0)^{1-\beta}}, \tag{4}$$

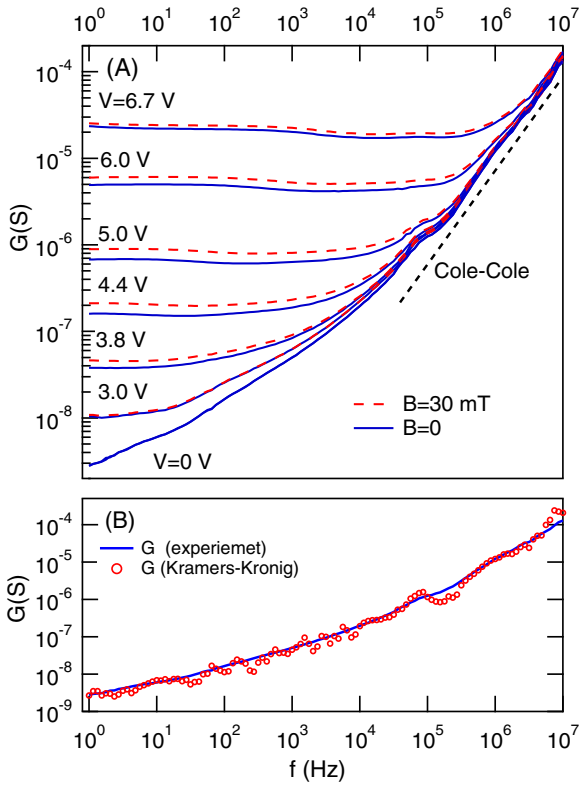

FIG. 4. (a) Differential conductance, G, as a function of frequency at indicated bias voltages for bipolar device B, measured at $B = 0$ and 30 mT. The dashed line is an approximation using the Cole-Cole relation (Eq. (4)), which is down-shifted for clarity. (b) Same as (a) at $V = 0$. The blue line in (b) represents the measured $G(f)$, whereas the circles were obtained from the imaginary part of the admittance using the Kramers-Kronig relation (see Eq. (5)).

where β is the "dispersion parameter" and τ_0 is the dipoles' mean relaxation time. Using Eq. (4), the high frequency conductance response is calculated to be $G(\omega) = \omega Im(\varepsilon(\omega))A/d$ where $A = 0.9$ mm^2 is the device area and $d = 150$ nm is its thickness. This approximation matches our data well. It is shown in Fig. 4(a) as a dashed line, which is downshifted for clarity. The best fitting parameters for this approximation are: $\varepsilon_s - \varepsilon_\infty = 0.4$, $\beta = 0.8$, and $\tau_0 = 0.5$ ns. Also from the value of the capacitance at high frequency we estimate $\varepsilon_\infty = 2.5$. At $f < 100$ kHz, the experimental conductance exceeds the estimated value from the Cole-Cole model; this indicates the presence of additional physical processes that contribute to the conductance at low frequency. Indeed, the *capacitance* response at zero voltage (Fig. 6) reveals a strong positive frequency-dependent contribution. This contribution is typically associated with the presence of trap states in the active material.[10] The admittance real and imaginary components are related to each other via the Kramers-Kronig relation. From the capacitance response versus frequency at zero bias (Fig. 6), we calculated the KK conductance, $G_{KK}(\omega)$, using an approximate form of the Kramers-Kronig (KK) relation (Eq. (9.43) in Ref. 23),

$$\varepsilon''(\omega) = -\frac{\pi}{2}\frac{d\varepsilon'(\omega)}{d(ln(\omega))}. \quad (5)$$

$G_{KK}(\omega)$ agrees rather well with the experimentally measured conductance (Fig. 4(b)), and this confirms the overall consistency of our measurements. This observation also points out that the low-frequency $G(\omega)$ and $C(\omega)$ responses at zero bias comes from the same physical process, which is related to trap states.[10]

The characteristic frequency dependence of the conductance at non-zero bias can be reasonably explained using $V_B = 6$ V as an example. The conductance stays fairly constant up to $f = 500$ kHz. Then, it increases slightly and merges with the dependence of $G(\omega)$ at zero bias. At frequencies above 1 MHz, the conductance at $V_B = 6$ V and $V_B = 0$ V is the same. The reason for that is that at high frequencies the contribution from the injected carriers is not important and $G(\omega)$ is dominated by the relaxation processes that are likely related to the relaxation of permanent dipoles;[22] however, the exact origin of this contribution is not important for our conclusions.

The OMAR effect in our device is relatively large, and thus the difference between $G(\omega)$ at $B = 0$ and $B = 30$ mT can be easily observed in Fig. 4(a). From these data, we extract the magnetoconductance $MG(\omega)$ at $B = 30$ mT versus frequency, which is shown in Fig. 5. $MG(\omega)$ has a characteristic frequency cutoff that shifts to higher frequencies with increasing bias voltage. As shown in Fig. 5(a) for the highest bias voltage (6.7 V) we were able to detect sizable (4.5%) $MG(\omega)$ even at frequency of 10 MHz. We did not find any correlation between the cutoff and the transient times of carriers in the bipolar devices. For example, using the data for the field-dependent mobility in MEH-PPV provided by Bozano *et al.*,[24] we estimated that the transient time for holes in device B is 100 μs for bias voltage $V_B = 4.8$ V and 32 μs for $V_B = 6.7$ V. The estimated transient time for electrons is

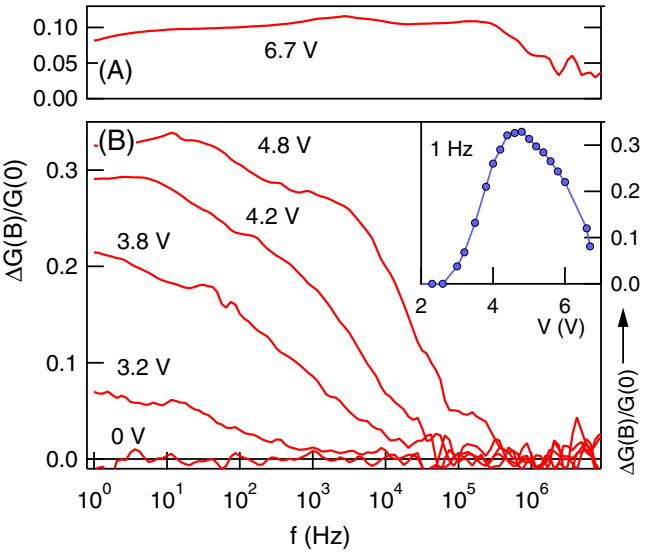

FIG. 5. The magnetoconductance, $MG(\omega)$, of device B measured at $B = 30$ mT, as a function of frequency at several bias voltages as indicated, extracted from the data in Fig. 4. The inset in panel (b) shows the dependence of MG at frequency $f = 1$ Hz on the bias voltage.

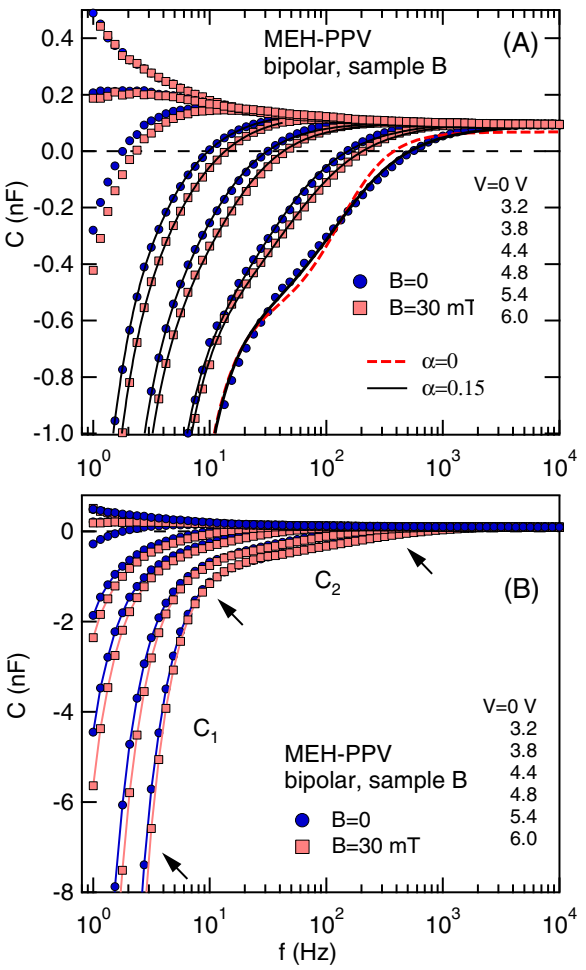

FIG. 6. (a) Differential capacitance versus frequency at the magnetic field $B = 0$ and $B = 30$ mT for device B at indicated voltages. The dashed line is a fit to the theoretical model with the dispersive parameter α set to zero, whereas the solid lines are fits with α as a free parameter. (b) Same data as in panel (a) in an expanded scale. The arrows indicate regions where contributions C_1 and C_2 dominate (see text).

270 μs for $V_B = 4.8$ V and 60 μs for $V_B = 6.7$ V. On the other hand, if we choose to characterize the $MG(\omega)$ cutoff by the frequency at which the magnitude of $MG(\omega)$ drops by half we find that the characteristic MG time-scale is 65 μs for $V_B = 4.8$ V and 1 μs $V_B = 6.7$ V.

We believe that the cutoff does not represent any process associated with the OMAR effect itself. It simply occurs, as we argued above, because at high frequencies the device conductance is dominated by processes that do not involve injected carriers. In fact, we will show below that peculiar frequency dependence of magnetoconductance can be quantitatively modeled by several relaxation processes that take place in MEH-PPV. These processes can be more easily identified from analysis of the imaginary part of admittance.

In Fig. 6(a), we show the dependence of the differential capacitance as a function of frequency in magnetic fields of 0 and 30 mT for bipolar device B; Fig. 6(b) shows the same data with an expanded vertical scale. At frequencies above 10 kHz, the capacitance does not depend on voltage or frequency; it is in fact equal to the "geometrical" capacitance, C_0. The behavior at $f < 10$ kHz, however, is much richer. At zero bias $C(\omega)$ is positive and increases with decreasing frequency. The positive contribution is typically associated with the presence of trap states in the active layer.[10] However, upon increasing the bias a negative contribution to the capacitance starts to develop, and shifts to higher frequencies with V_B. In this regime, the capacitance also reveals a dependence on the magnetic field. Several processes have been proposed to explain the strong negative capacitance in organic diodes at $V_B > V_{BI}$. These are (i) bimolecular recombination,[25,26] (ii) trap-assisted monomolecular recombination,[27] (iii) electron injection through interfacial states.[28] Since in principle all three processes can take place in our devices, we only phenomenological analyze the data.

Inspection of $C(f)$ measured at $V_B = 6$ V shown in Fig. 6(b) suggests that there are two contributions to the negative capacitance. The high frequency contribution, C_2 dominates in the frequency range 10 Hz $< f <$ 1 kHz; whereas the low frequency contribution, C_1 dominates at $f <$ 10 Hz. To verify this picture, we show in Fig. 7 the data for device B at $V_B = 4.4$ V and 6 V in a $-Z''(\omega)$ versus $Z'(\omega)$ plot (the Cole-Cole plot), where Z'' and Z' are the imaginary and real part of the device impedance, respectively. For both biases the low-frequency part of the Cole-Cole plot shows a characteristic bend. The change in the curvature of the Cole-Cole curve suggests an additional process with distinct time constant.[29]

The admittance response versus frequency and the emergence of negative capacitance can be related to the time domain response of the system to an instantaneous voltage step ΔV.[30] It was shown that if the derivative of a transient current, dj_r/dt is positive, then the capacitance $C(\omega)$ is smaller than the geometrical capacitance, $C_0 = \varepsilon_r \varepsilon_0 A/d$, and may be actually negative. In a simple case, when a transient current relaxes exponentially in time as $j_r(t) = -j_0 \exp(-t/\tau)$ with $j_0 > 0$, the admittance acquires an additional contribution,

$$Y_r(\omega) = \frac{i\omega}{\Delta V}\int_0^\infty j_r(t)\,\exp(-i\omega t)dt = -\frac{i\omega j_0 \tau}{\Delta V(1+i\omega\tau)}. \quad (6)$$

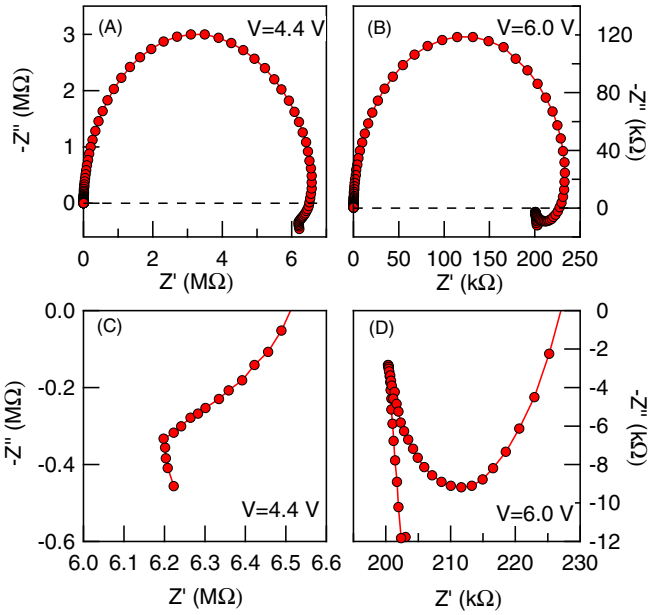

FIG. 7. The Cole-Cole plot of $-Z''(\omega)$ vs. $Z'(\omega)$ for the bipolar device B at bias voltage V = 4.4 V (panel (a)) and V = 6 V (panel (b)). Panels (c) and (d) emphasize the low frequency regions of (a) and (b), respectively.

Then, the conductance $G(\omega)$ and capacitance $C(\omega)$ become

$$G(\omega) = G_0 - \frac{j_0\tau^2\omega^2}{\Delta V(1+\omega^2\tau^2)}, \quad (7)$$

$$C(\omega) = C_0 - \frac{j_0\tau}{\Delta V(1+\omega^2\tau^2)}, \quad (8)$$

where G_0 is the DC or steady state conductance.

We used a single exponential transient term to approximate C_1, the low-frequency contribution to the capacitance. To take into account a possible distribution of relaxation times for the high-frequency contribution we introduced phenomenological parameter α. The resulting equation used for fitting the capacitance data is

$$C(\omega) = C_0 - C_{10}\frac{1}{1+\omega^2\tau_1^2} - C_{20}\mathrm{Re}\left[\frac{1}{1+(i\omega\tau_2)^{1-\alpha}}\right], \quad (9)$$

where $C_{10}, C_{20}, \tau_1, \tau_2$, and α are fitting parameters that characterize the two contributions to the negative capacitance. The fits shown in Fig. 6(a) agree with the experimental data quite well. For the capacitance at $V_b = 6$ V, the dashed red line displays a fit obtained with $\alpha = 0$, which corresponds to the description of the high-frequency contribution having a single exponential transient term. We found that whereas incorporation of α as a free parameter clearly improves the agreement with the data, it only slightly affects the values of the other fitting parameters.

From fitting the data in the range $4.4 < V_B < 6$ V, we found that the time constant $\tau_1 \approx 0.8$ s, $C_{20} \approx 0.6$ nF and $\alpha \approx 0.15$ do not have any systematic dependence on the bias voltage. Remarkably, the behavior of C_{10} and τ_2 shown in Fig. 8 is very different. Both quantities change exponentially with the bias; the former grows as $C_{10} \sim \exp(\gamma V_b)$ and the

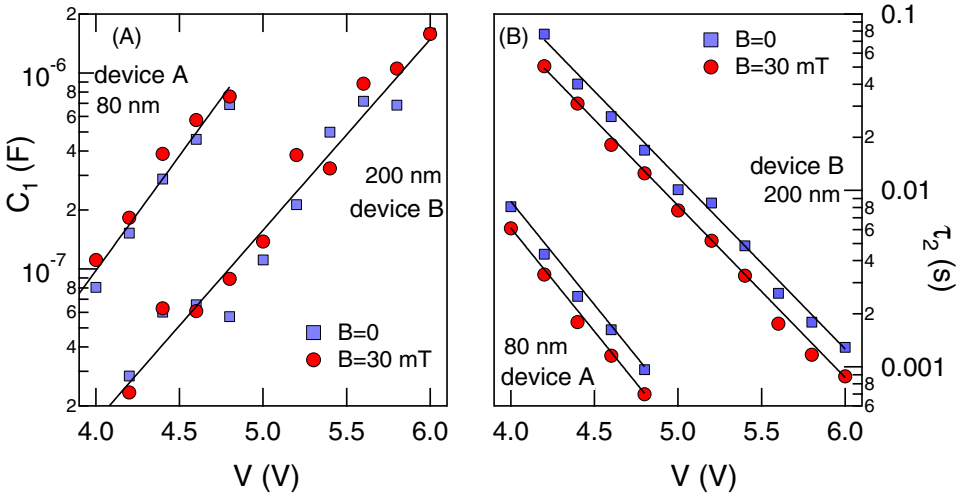

FIG. 8. The dependence of the fitting parameters, C_{10} (a) and τ_2 (b) as a function of bias voltage for devices B and A.

later decreases as $\tau_2 \sim \exp(-\gamma V_b)$. The parameter $\gamma = 2.25\ \mathrm{V}^{-1}$ turned out to be the same in both dependencies.

Alongside with devices B discussed above, we also analyzed the admittance for device A that has smaller thickness of 80 nm. The parameters C_{10} and τ_2 for this device are shown in Fig. 8. They also depend exponentially on the bias voltage; but the curves are shifted to low voltages with respect to device B; the parameter $\gamma = 2.7\ \mathrm{V}^{-1}$ again is the same for C_{10} and τ_2 functional dependencies.

The life-time of excess carriers for bimolecular recombination (BMR) kinetics may be written as $\tau_{BM}^{-1} \approx \lambda\langle n\rangle$, where $\lambda = \langle v\rangle\sigma_R$, $\langle v\rangle$ is the relative velocity of negative and positive polarons, σ_R is their recombination cross section, and $\langle n\rangle$ is an average concentration of carriers.[18] From this relation, we expect that τ_{BM}^{-1} depends strongly on the carrier concentration and correspondingly on the bias voltage – behavior that is clearly displayed by the time constant τ_2. If we assume that the bias dependence of τ_2 comes from the increase in the carrier density, we can also explain why parameter C_{20} does not depend on the bias voltage. From Eqs. (7) and (9), we have $C_{20} = j_{20}\tau_2/\Delta V$ where j_{20} is a magnitude of the relaxation current for the fast process at $t = 0$, immediately after application of a voltage step ΔV. j_{20} is expected to be directly proportional to the carrier concentration $\langle n\rangle$. Because $\tau_2 \sim \langle n\rangle^{-1}$, the two dependencies cancel each other, and hence the parameter C_{20} is expected to be bias-independent.

From Fig. 8, it can be clearly seen that the application of magnetic field $B = 30$ mT decreases the time constant τ_2. The change of τ_2 is about 30%; it does not depend on bias voltage and remains the same for devices A and B. The electroluminescence (EL) in bipolar PPV-based devises is also strongly affected by magnetic field.[9] The BMR parameter λ does not depend on the bias voltage but is affected by the applied magnetic field as was suggested in the polaron-pair model of the OMAR effect.[6] The similarity in the magnetic field response and strong dependence of τ_2 on bias voltage (i.e., on the carrier density) suggest that C_2 contribution originates from the bimolecular recombination and τ_2 is the carrier life-time associated with this process. This conclusion is indirectly supported by our admittance measurements of unipolar device E. In this device, as shown in Fig. 9, the high frequency contribution C_2 is not present at all and the effect of magnetic field is not detected.

This interpretation can be further confirmed by plotting the inverse of the relaxation time τ_2 as a function of voltage alongside with the dependence of the current on the bias voltage, as it is shown in the Fig. 10. We observe that both quantities have the same functional dependence on bias voltage in the range between 4 and 6 V. The concurrence of the data can be simply related to the fact that both the DC current and τ_{BM}^{-1} are directly proportional to the carrier density $\langle n\rangle$. Exact reason for the roughly exponential $I(V)$ characteristic between 4 and 6 V is not clear. Possibly, it is related to a blocking contact or a continuous filling of trap states in the device with increasing voltage.

Let us now discuss the negative contribution C_1 that dominates capacitance for $f < 10$ Hz. Similar negative contribution, with a time constant weakly dependent on the bias voltage was recently observed in MDMO-PPV (Ref. 27) and in α-NPD.[31] In both cases, the negative capacitance was attributed to the trap-assisted monomolecular recombination. Moreover, for α-NPD this interpretation was confirmed by

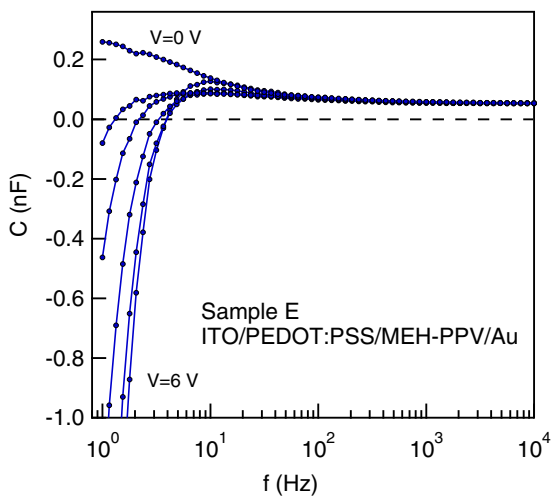

FIG. 9. Differential capacitance as a function of frequency for device E at several bias voltages between 0 and 6 V. The sequence of layers in the device is indicated. At low bias the device is unipolar. At higher biases injection of electrons from Au electrode is possible.

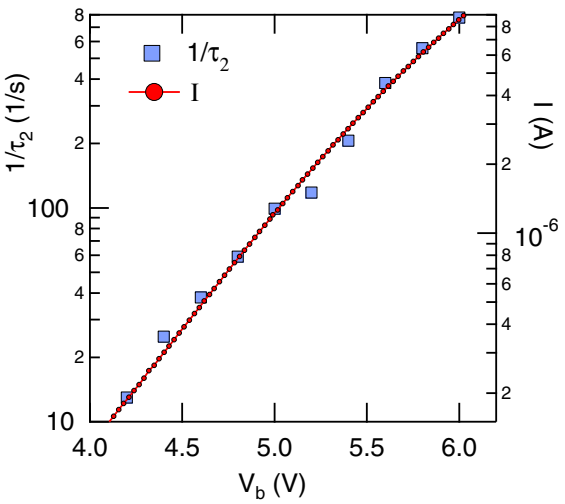

FIG. 10. The inverse of the relaxation time τ_2 as a function of the bias voltage (left axis) alongside with the DC current versus bias voltage (right axis).

numerical simulations that showed that the low frequency negative capacitance occurs when a band of defects is present, and both electrons and holes are injected. It is likely that in our MEH-PPV devices the low frequency term also stems from volume trap-assisted recombination. This interpretation allows to understand why the magnitude of the term, C_{10}, has the same dependence on voltage as the $1/\tau_2$ and DC current. From Eq. (8), we have $C_{10} = j_{10}\tau_1/\Delta V$; since for the trap-assisted recombination it is expected that τ_1 is constant, the C_{10} is determined by the magnitude of the relaxation current j_{10}, which as well as the DC current and $1/\tau_2$ is determined by the carrier concentration. Thus, the attribution of C_1 term to the trap-assisted recombination and C_2 term to the bimolecular recombination gives mutually consistent explanation for our DC and AC data.

Recently trap-assisted recombination of electrons and holes was studied in MEH-PPV (Ref. 32) by transport measurements and numerical simulations. It was demonstrated that the rate limiting step for this process is the diffusion of holes towards trapped electrons. The hole capture coefficient was estimated to be $C_p = 9.0 \times 10^{-19}$ m^3 s,[33] and the trap density $N_t = 1.1 \times 10^{23}$ m^{-3}.[17] With these values the carriers lifetime associated with this process was calculated to be $\tau_{tr} = (N_t C_p)^{-1} = 10$ μs, which is much smaller than the experimentally observed lifetime of 0.8 s in the present studies. The reason for such disagreement is not understood.

A different interpretation of the negative capacitance was recently proposed to explain the behavior of the admittance in PPV co-polymer "super yellow."[28] In this work, the negative capacitance was attributed to the sequential electron injection at the organic/metal interface. Intermediate states were attributed to a dipole layer at the interface between PPV and Ba electrode, which was used as a cathode material in this work. This mechanism could explain the C_1 term in our bipolar MEH-PPV devices, where a dipole layer can be formed at the PPV/Ca interface. However, as it is shown in Fig. 9, the low-frequency negative capacitance was also detected in unipolar device E, where gold was used as a cathode material. In the unipolar device at $V_b = 6$ V the negative capacitance term has the same time constant $\tau_2 = 0.8$ s as in the bipolar device, but its magnitude is about 100 times smaller than C_{10} in bipolar device B at the same bias. In fact the behavior of the unipolar device can be better understood within the trap-assisted recombination assuming that at sufficiently high bias electrons are directly injected into localized trap states. Within this mechanism the trap assisted recombination is confined to a narrow layer of PPV adjacent to the cathode, and consequently is expected to produce a much smaller contribution to the negative capacitance. The life time is still determined by the hole capture and is expected to be the same as in bipolar devices.

Full description of the processes responsible for the C_1 contribution should incorporate the experimental observation that this process is affected by magnetic field as shown in Fig. 6. From the fit to the data, we could not establish which of the two parameters, C_{10} or τ_1 changes upon the application of a magnetic field. We found that if both parameters are allowed to be free during the fitting procedure, no clear dependence on magnetic field can be observed, as is shown, for example, in Fig. 8(a) for the capacitance C_{10}. However, if any of the two parameters was held constant, then the other parameter showed a systematic response to magnetic field.

The appearance of relaxation terms in the differential capacitance has to be accompanied by corresponding terms in the device differential conductance. From Eqs. (6), (8), and (9), we found that the conductance of our bipolar devices is expected to follow the dependence,

$$G(\omega) = G_0 - C_{10}\frac{\omega^2\tau_1}{1+\omega^2\tau_1^2} + C_{20}\,\mathrm{Im}\left[\frac{\omega}{1+(i\omega\tau_2)^{1-\alpha}}\right] + G_{CC}, \tag{10}$$

where in addition to the first three terms related to the injected carriers we added G_{CC}, the Cole-Cole contribution to the AC conductance. In Fig. 11(a), we show the conductance data for device B at bias voltage 6 V in the magnetic fields of 0 and 30 mT. Solid lines display the fit of $G(f)$ dependence with Eq. (10). In fact to obtain these fits, we adjusted only one parameter, G_0, that represents the steady state DC conductance. With the model, G_0 does not depend on frequency but can depend on magnetic field. For $C_{01}, C_{02}, \tau_1, \tau_2$, and α, we used the values obtained from the fitting of the capacitance data and for G_{CC}, the dependence at zero bias was used. (This dependence is shown in Fig. 4(a) as the dashed line.) The agreement with the experimental data is quite good. The deviation between the theory and experiment around frequency $f = 10^5$ Hz can be associated with a small peak in the conductance data that are present in $G(f)$ at all bias voltages (see Fig. 4(a)) and that was not included in Eq. (10). Using theoretical curves for $G(f)$ dependencies in magnetic fields of 0 and 30 mT, we computed theoretical dependence for magnetoconductance $MG(f)$. As shown in Fig. 11(b), this dependence gives good approximation for experimental variation of magnetoconductance. In particular, the theory reproduces a small broad peak with the center at $f \approx 300$ Hz, that occurs because the relaxation time τ_2 has different values in zero magnetic field,

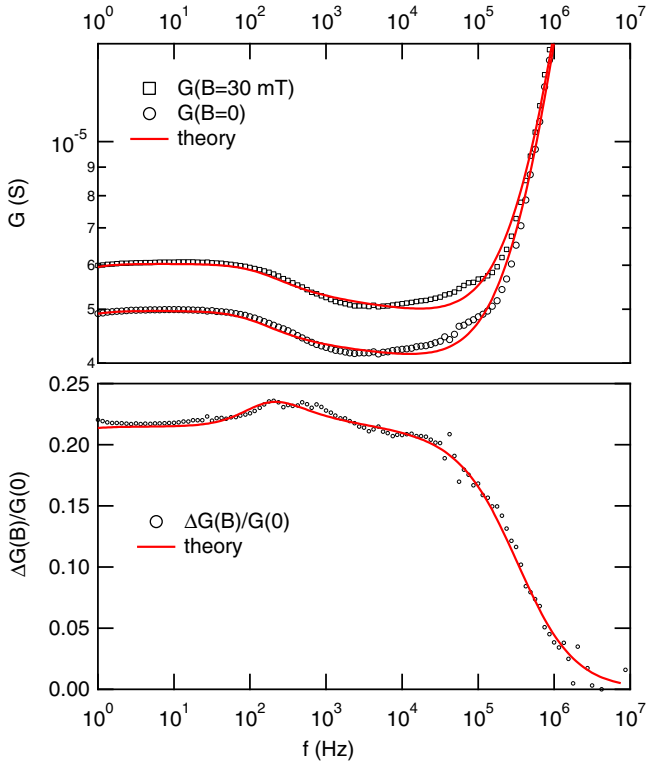

FIG. 11. (a) Differential conductance as a function of frequency for device B at $V_B = 6$ V and indicated magnetic fields. The solid red line is a fit to Eq. (10). (b) The magnetoconductance, $MG(\omega)$, of device B measured at $B = 30$ mT, as a function of frequency at $V_B = 6$ V. The solid red line shows the theoretically expected $MG(\omega)$ variation.

$\tau_2 = 1.2$ ms, and in $B = 30$ mT, $\tau_2 = 0.9$ ms. The cutoff of the magnetoresistance is also well approximated and can be related to the magnetic-field-independent Cole-Cole contribution to the conductance.

Our extensive set of conductance data allows to make another interesting observation. In Figs. 12 and 13, respectively, we plotted experimental magnetoconductance and magnetocapacitance of device B as a function of frequency. The data were taken in magnetic field $B = 30$ mT; panels (a) and (b) of the figures represent data for two bias voltages, 4.2 and 5.8 V, respectively. In addition, in the figures we superimposed scaled normalized derivatives of conductance, ΔG_S, and capacitance, ΔC_S, defined as

$$\Delta G_S(f) = [G(V_1,f) - G(V_0,f)]/G(V_0,f)/S, \qquad (11a)$$

$$\Delta C_S(f) = [C(V_1,f) - C(V_0,f)]/C(V_0,f)/S, \qquad (11b)$$

where $G(V,f)$ and $C(V,f)$ are experimentally measured conductance and capacitance in *zero magnetic field* and S is an adjustable scaling coefficient. For bias voltage $V = 4.2$ V, we used *experimental* data for capacitance and conductance at $V_0 = 4.2$ V and $V_1 = 4.4$ V. We found that the same scaling coefficient $S = 2.1$ brings the conductance data, $MG(f)$ and $\Delta G_S(f)$ (Fig. 12(a)), and the capacitance data, $MC(f)$ and $\Delta C_S(f)$ (Fig. 13(a)) in almost exact agreement. Equally good agreement was obtained for bias voltage $V = 5.8$ V, where we used data for $V_0 = 5.8$ V and $V_1 = 6$ V and adjusted scaling coefficient to $S = 1.75$ (Figs. 13(b)). Similar agreement

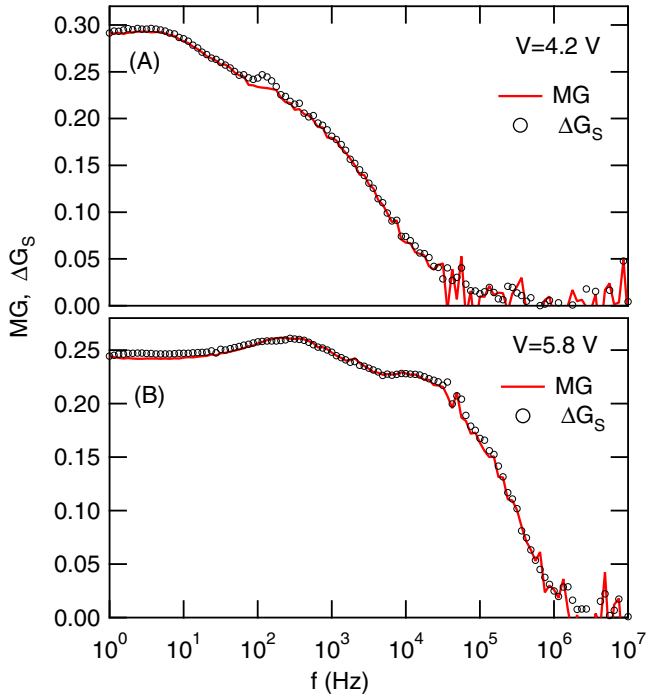

FIG. 12. Magnetoconductance, MG, and the scaled normalized derivative of the conductance at zero field, ΔG_S, as function of frequency for device B at the bias voltage 4.2 V (a) and 5.8 V (b).

was observed at other bias voltages. We emphasize that the figures display not theoretical fits; two curves in each panel represent experimental data, one reflecting the response of the device on application of magnetic field and another on small increase in the bias voltage. Both curves account for peculiar frequency variation of the device admittance. For example, at $V_B = 5.8$ V both $MG(f)$ and $\Delta G_S(f)$ reproduce a broad peak with the center at $f = 300$ Hz related to the change of time constant τ_2 with magnetic field or bias

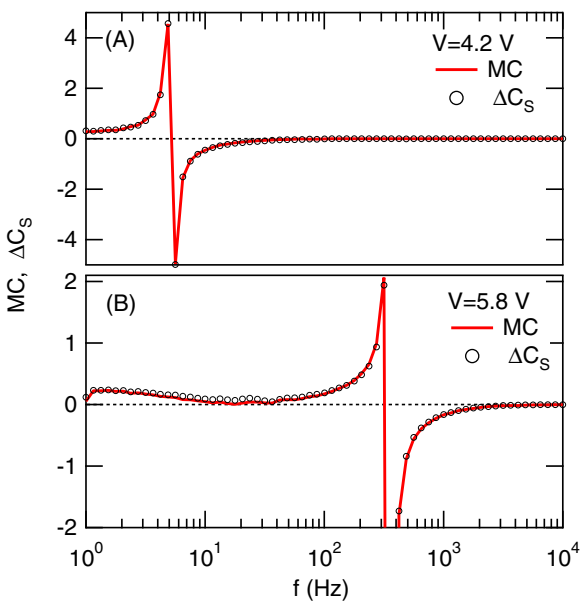

FIG. 13. Magnetocapacitance, MC, and the scaled normalized derivative of the capacitance at zero field, ΔC_S, as function of frequency for device B at the bias voltage 4.2 V (a) and 5.8 V (b).

voltage (Fig. 12(b)) and at $V_B = 4.2\,\mathrm{V}$ both $MC(f)$ and $\Delta C_S(f)$ show discontinuity at $f = 4.6\,\mathrm{Hz}$ related to the fact that at this frequency the capacitance of the devices changes from negative to positive (Fig. 13(a)). Summarizing our observation, we can conclude that in the bias range where admittance depends on magnetic field the frequency-dependent response of the device to a small magnetic field is equivalent to the response to a small increase in the bias voltage in *zero magnetic field*.

SUMMARY

In summary, we studied high frequency electronic transport in several bipolar and unipolar MEH-PPV based OLEDs by means of admittance spectroscopy. We found that the differential capacitance of bipolar devices contains two negative contributions that are affected by the magnetic field. The first contribution that dominates at frequencies below 10 Hz is likely associated with trap-assisted recombination. The second contribution, which is associated with the bimolecular electron-hole recombination, dominates the negative capacitance above 10 Hz. We found that its time constant, τ_2, exponentially decreases with the bias voltage. Application of a magnetic field $B = 30\,\mathrm{mT}$ decreases τ_2 by 30%. We also found that the magnetoconductance response versus frequency has a characteristic cutoff that shifts to higher frequencies with increasing bias. The reason for this behavior is that at high frequencies any conductive processes associated with injected carries is shorted by the dissipative processes that are present in unbiased samples. These high-frequency processes are likely related to the depolarization of permanent dipoles. For one of the devices we observed that the conductance at 10 MHz was enhanced by 4.5% when a magnetic field $B = 30\,\mathrm{mT}$ was applied. We also found that the frequency-dependent response of the device to a small magnetic field is equivalent to the response to a small increase in the bias voltage in zero magnetic field.

ACKNOWLEDGMENTS

The authors would like to thank C. Boehme, T. D. Nguyen, and Z. V. Vardeny for valuable comments and discussions. This work was supported by NSF CAREER Grant No. DMR 0955484, and the NSF-MRSEC program at the University of Utah, Grant No. DMR 11-21252.

[1]T. L. Francis, O. Mermer, G. Veeraraghavan, and M. Wohlgenannt, New J. Phys. **6**, 185 (2004).
[2]O. Mermer *et al.*, Phys. Rev. B **72**, 205202 (2005).
[3]Y. Iwasaki *et al.*, Phys. Rev. B **74**, 195209 (2006).
[4]T. D. Nguyen, B. R. Gautam, E. Ehrenfreund, and Z. V. Vardeny, Phys. Rev. Lett. **105**, 166804 (2010).
[5]P. A. Bobbert, T. D. Nguyen, F. W. A. van Oost, B. Koopmans, and M. Wohlgenannt, Phys. Rev. Lett. **99**, 216801 (2007).
[6]V. N. Prigodin, J. D. Bergeson, D. M. Lincoln, and A. J. Epstein, Synth. Met. **156**, 757 (2006).
[7]J. D. Bergerson, V. N. Prigodin, D. M. Lincoln, and A. J. Epstein, Phys. Rev. Lett. **100**, 067201 (2008).
[8]P. Desai *et al.*, Phys. Rev. B **75**, 094423 (2007).
[9]T. D. Nguyen *et al.*, Nature Mater. **9**, 345 (2011).
[10]W. Wagemans, P. Janssen, E. H. M. van der Heijden, M. Kamerink, and B. Koopmans, Appl. Phys. Lett. **97**, 123301 (2010).
[11]F. Wang *et al.*, Synth. Met. **161**, 622 (2011).
[12]F. Li, L. Xin, S. Liu, and B. Hu, Appl. Phys. Lett. **97**, 073301 (2010).
[13]R. Richet, Rev. Sci. Instrum. **67**, 3217 (1996).
[14]I. H. Campbell, T. W. Hagler, D. L. Smith, and J. P. Ferraris, Phys. Rev. Lett. **76**, 1900 (1996).
[15]Y.-J. Lin *et al.*, Appl. Phys. Lett. **91**, 092127 (2007).
[16]P. Kumar, S. C. Jain, A. Misra, M. N. Kamalasanan, and V. Kumar, J. Appl. Phys. **100**, 114506 (2006).
[17]N. T. Nikolai, M. M. Mandoc, and P. W. M. Blom, Phys. Rev. Lett. **83**, 165204 (2011).
[18]K. C. Kao and W. Hwang, *Electrical Transport in Solids* (Pergamon, Oxford, 1981).
[19]W. J. Baker, D. R. McCamey, K. J. van Schooten, J. M. Lupton, and C. Boehme, Phys. Rev. B **84**, 165205 (2011).
[20]F. J. Wang, H. Bassler, and Z. V. Vardeny, Phys. Rev. Lett. **101**, 236805 (2008).
[21]H. C. F. Martens, H. B. Brom, and P. W. M. Blom, Phys. Rev. B **60**, R8489 (1999).
[22]G. R. Strobl, *The Physics of Polymers: Concepts for Understanding Their Structures and Behavior* (Springer, Berlin, 1997), Chap. 5.
[23]C. J. F. Bottcher and P. Bordewijk, *Theory of Electric Polarization* (Elsevier, Amsterdam, 1978), Vol. 2.
[24]L. Bozano, S. A. Carter, J. C. Scott, G. G. Malliaras, and P. J. Brock, Appl. Phys. Lett. **74**, 1132 (1999).
[25]H. H. P. Gommans, M. Kemerink, and R. A. J. Janssen, Phys. Rev. B **72**, 235204 (2005).
[26]C. Lungenschmied, E. Ehrenfreund, and N. S. Saricifci, Org. Electron. **10**, 115 (2009).
[27]E. Ehrenfreund, C. Lungenschmied, G. Dennler, H. Neugebauer, and N. S. Saricifci, Appl. Phys. Lett. **91**, 012112 (2007).
[28]J. Bisquert, G. Garcia-Belmonte, A. Pitarch, and H. J. Bolink, Chem. Phys. Lett. **422**, 184 (2006).
[29]*Impedance Spectroscopy Theory, Experiment and Application*, edited by E. Barsoukov and J. R. Macdonald (Wiley-Interscience, New Jersey, 2005).
[30]M. Ershov *et al.*, IEEE Trans. Electron Devices **45**, 2196 (1998).
[31]N. D. Nguyen, M. Schmeits, and H. P. Loebl, Phys. Rev. B **75**, 075307 (2007).
[32]M. Kuik, L. J. A. Koster, G. A. H. Wetzelear, and P. W. M. Blom, Phys. Rev. Lett. **107**, 256805 (2011).
[33]M. Kuik *et al.*, Appl. Phys. Lett. **98**, 093301 (2011).